

We are IntechOpen, the world's leading publisher of Open Access books Built by scientists, for scientists

4,800

Open access books available

122,000

International authors and editors

135M

Downloads

Our authors are among the

154

Countries delivered to

TOP 1%

most cited scientists

12.2%

Contributors from top 500 universities



WEB OF SCIENCE™

Selection of our books indexed in the Book Citation Index
in Web of Science™ Core Collection (BKCI)

Interested in publishing with us?
Contact book.department@intechopen.com

Numbers displayed above are based on latest data collected.
For more information visit www.intechopen.com



Combined Transmission Electron Microscopy – *In situ* Measurements of Physical and Mechanical Properties of Nanometer-sized Single-phase Metallic structure

Hideki Masuda

Additional information is available at the end of the chapter

<http://dx.doi.org/10.5772/60750>

Abstract

This chapter reviews the results of silver nanometer-sized contacts (Ag NCs). To realize fabrication, atomistic observation, and mechanical and electrical measurement of Ag NCs, an *in situ* method where a contact-retract test of atomic force microscopy and a current feedback function of scanning tunnelling microscopy have been combined with high-resolution transmission electron microscopy (HRTEM). By inserting these functions inside HRTEM, it has been enabled to observe atomistic structures, which can be formed at the final stage of a rapture process, and to measure a change of properties correlated to structural dynamics.

Keywords: Silver nanometer-sized contacts, atomic force microscopy, conductance quantization, Young's modulus

1. Introduction

Currently, miniaturisation of electronics has continued, and it started the device development at atomistic and molecular scale.[1] Devices included into this electronic circuit are nanometer-sized contacts (NCs), atomic-sized wires (ASWs), single molecular junctions (SMJs), and so on. [2] (Figure 1) SMJ is a system of a single molecule sandwiched by a pair of nanometer-sized metallic electrodes. SMJs enable single electronic operation, high-density integration, and electric power saving.[3-7] To engineer SMJs, we need to reveal structure of device configu-

ration that includes interfaces between molecules and electrodes and mechanical and electrical properties. Metallic NCs and ASWs are fundamental materials that have potentials for device applications themselves as well as key factors of application for SMJs[8].

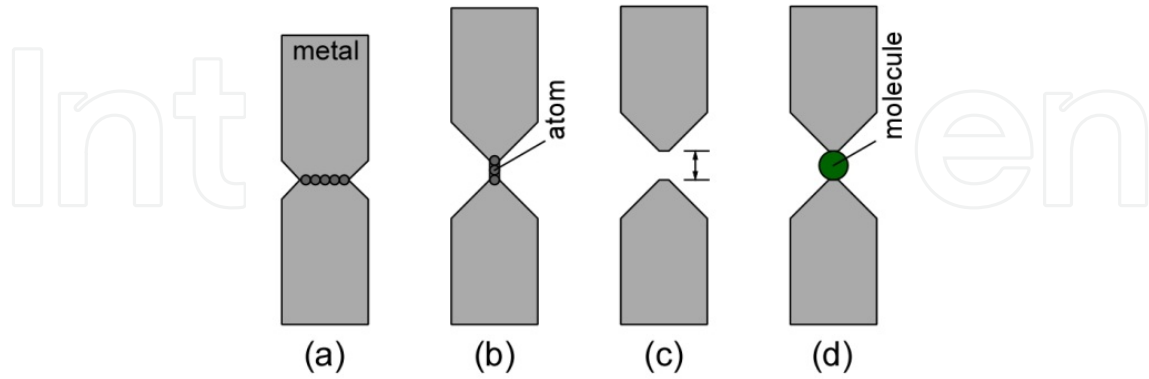


Figure 1. Schematics of atomistic scale devices. (a) NC, (b) ASW, (c) nano-gap structure, and (d) SMJ.

1.1. Electrical Property of NCs

Research in metallic NCs at 1988 by van Wees et al. started with conductance quantization in a point contact of two-dimensional electronic gas (2DEG) formed at interface of semiconductors. [9] When a negative bias is applied between gate electrodes placed on semiconductors, a depletion layer is formed in 2DEG under the electrodes. At a gap of this depletion layer, in which electrons cannot exist, a point contact of 2DEG forms. Energy of electrons passing through the contact is written as below, wherein W is the width of point contact.

$$E = \frac{\hbar^2 k_x^2}{2m} + \frac{\hbar^2}{2m} \left(\frac{\pi n_y}{W} \right)^2 \quad (n_y = 1, 2, 3, \dots) \quad (1)$$

Here, the first term is the kinetic energy along x direction, and the second term is the discrete energy level due to confinement along y direction. With n_y of the second term, one-dimensional sub-band is formed (Figure 2). The cross-point of sub-band and Fermi-level (E_F) correspond to one conductive channel. When you increase bias voltages applied to gate electrodes, the area of depletion layer becomes wider and the width of electrons passing through becomes narrower. The second term is inversely proportional to square of W ; N decreases with decrement of W . In the experiment conducted by van Wees et al., the length of conductive channel was smaller than $0.3 \mu\text{m}$, and because this is shorter than the mean free path of electrons in 2DEG ($8 \mu\text{m}$), electrons show ballistic conduction in this system. As a resultant, conductance of point contact is written as below (Landauer formula).

$$G = \frac{2e^2}{h} \sum T_n \quad (2)$$

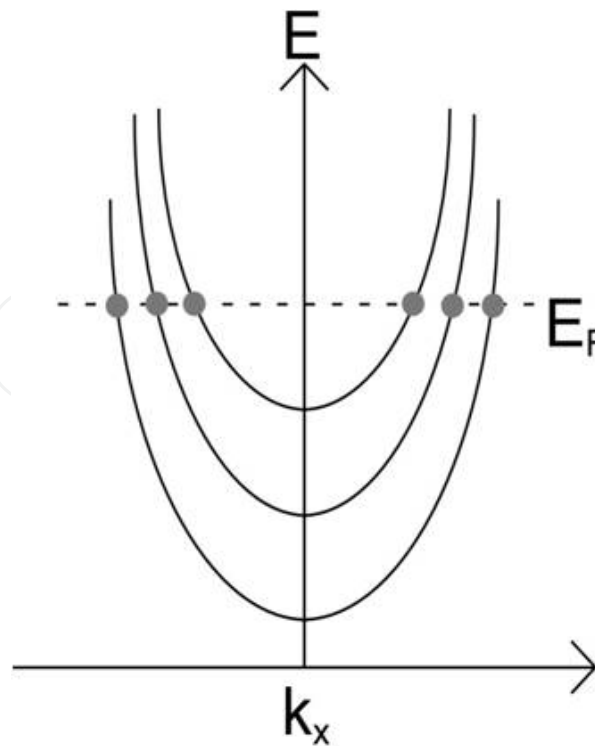


Figure 2. Schematic illustration of one-dimensional sub-band.

Here, T_n is the transmittance of an electron near the Fermi level (conductive channel), $2e^2/h$ ($= G_0$) is unit of quantization, e is charge of electron, and h is Plank's constant. Under assumption of ballistic conduction, transmittance of each conduction channel is $T_n = 1$; therefore, conductance of one conductive channel is $1 G_0$. When the width of point contact (W) changes, the conductance varies with steps of integer multiples of G_0 . That is, conductance quantization occurs when the length of electron conduction path becomes shorter than electron mean free path (ballistic conduction) and when the width of electron conduction path becomes narrow enough to count up the number of conductive channels. It is thought that this phenomenon also occurs in a system of metallic NCs, whose contact length is not so longer than electron mean free path.[10]

In early stage of metallic NCs, niobium (Nb) and nickel (Ni) NCs were researched. Just before the rupture of these NCs in tensile deformation process, the conductance of several G_0 is often observed.[11-15] This result triggered to relate the electrical conductance of metallic NCs to conductance quantization. Moreover, in gold (Au) or sodium (Na) NCs, a high probability of the conductance measured as integer multiples of G_0 is shown. [16-18] At that time, conductance of Au NCs varied in a staircase pattern (Figure 4). However, step height in this measurement is different from one time to another and not always corresponds to integer multiples of G_0 . To analyse these result statistically, conductance histograms were made through the accumulation of considerable conductance variation traces (Figure 5). In the histograms for Au and Na NCs (Figure 6), peaks appeared at integer multiples of G_0 .

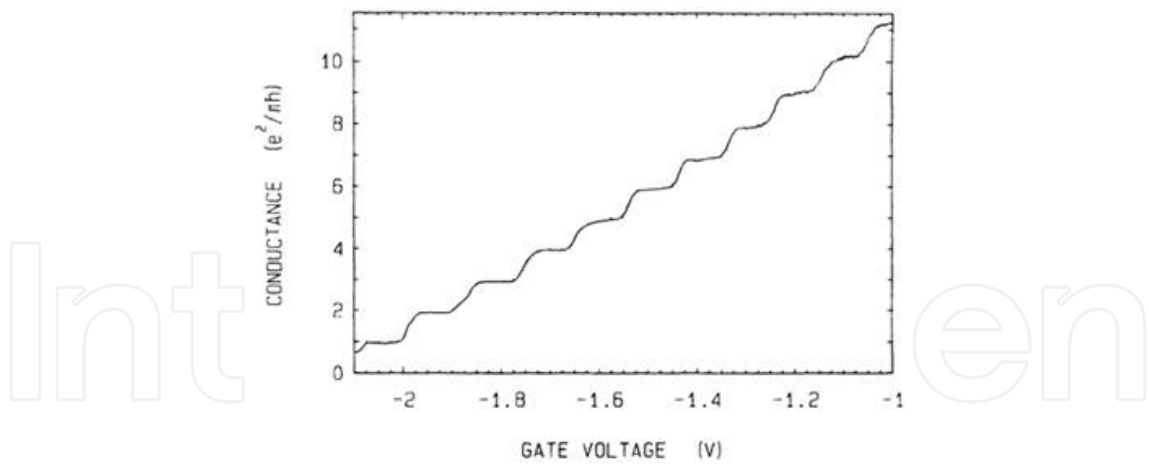


Figure 3. Conductance of 2DEG varies with gate voltage.[9]

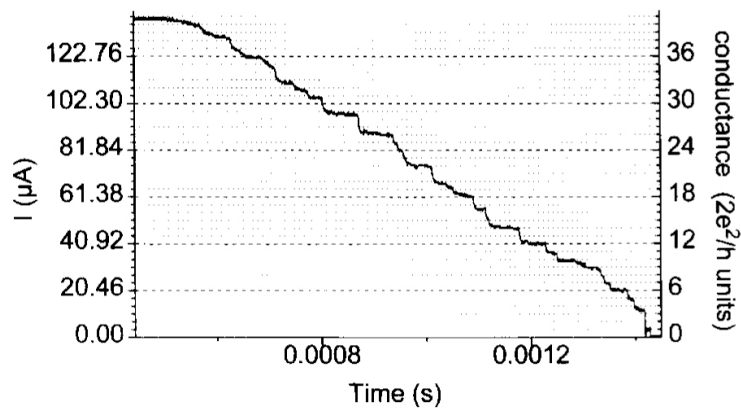


Figure 4. Time variation of conductance in tensile deformation process of Au NCs. [16]

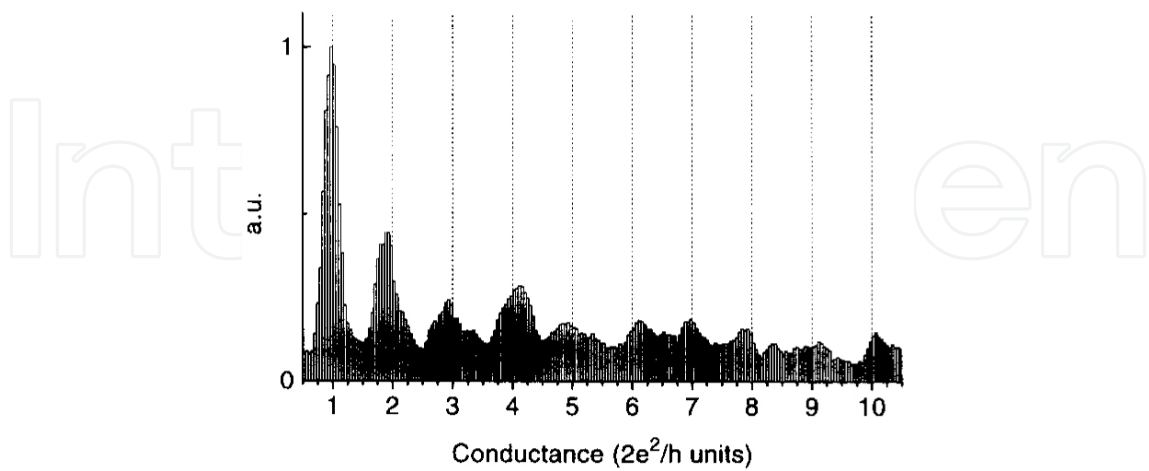


Figure 5. Conductance histogram of Au NCs. [16]

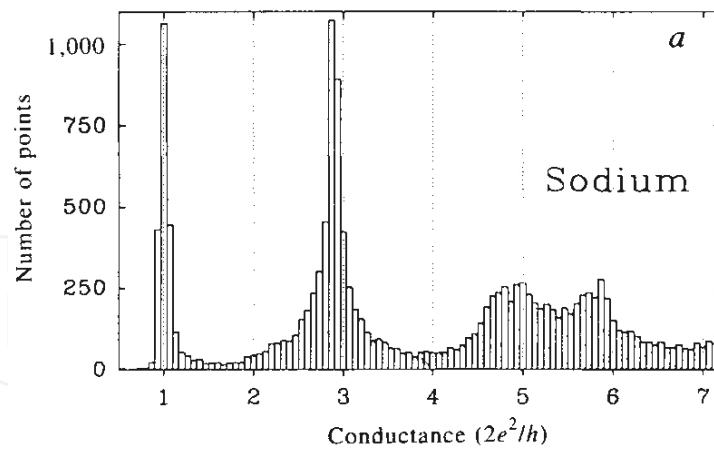


Figure 6. Conductance histogram of Na NCs. [16]

After the electrical conductance of NCs for other metallic species was researched, construable conductance of quantization was limited for monovalent metals, which are better suited for free electron approximation, such as Au[19, 20], silver (Ag) [19, 21-26], copper (Cu)[11, 19, 21, 27-35], and Na[18, 36, 37]. For the other metallic NCs, such as Nb[12, 13, 15, 21, 38], Ni[11, 14, 17, 22, 39-41], platinum (Pt) [11, 12, 17, 22, 28, 42-51], aluminium (Al), [13, 15, 28, 52, 53], paradium (Pd) [31, 44, 47, 49, 54, 55], iridium (Ir) [44, 46, 54], rhodium (Rh) [44, 54], zinc (Zn) [56, 57], and cobalt (Co)[47], the measured conductance is not construable for integer multiples of G_0 . In other words, conductance of metallic NCs is categorized into two main types as quantization and anti-quantization.

1.2. Structure of NCs

To fabricate metallic NCs, mechanically controllable break junction (MCBJ) method [12, 38] and STM method [58] were mainly used. In these methods, however, one cannot observe the structure of NCs. Therefore, for quantization-type NCs, it is expected that the minimum cross-sectional area of NC, which shows the integer multiples of G_0 , corresponds to the conductance using Landauer formula [59] and Sharvin's equation.[10, 60]

$$G_s = \frac{2e^2}{h} \left(\frac{k_F a}{2} \right)^2 \quad (3)$$

Here, k_F is Fermi wavelength of metals at room temperature, and a is the minimum cross-sectional radius. Objectively, the smallest structure that corresponds to the lowest step height of conductance staircase ($1 G_0$) is expected to be a single atom contact. Similarly, $2 G_0$ to two atoms contact, $3 G_0$ to three atoms contact, and so on; that is, a simple correspondence relation between the minimum cross-section area and the conductance of NCs is proposed. However, for Au NCs, direct observation using *in situ* HRTEM method show failure of this simple relationship.[61] For anti-quantization-type NCs, such relationship cannot be defined at all.

The structure should be directly observed to research a relationship between the structure and the conductance.

1.3. Mechanical property of NCs

Gimzewski et al. researched elastic and plastic deformation of NCs [62], but they could not discuss the mechanical properties of NCs by hitherto known MCBJ and STM methods. After that, Agraït et al. introduced the secondary STM tip on the backside of first tip to measure the displacement, and they also measured the conductance and force variation at the same time. [63] In 1996, Rubio et al. introduced an AFM cantilever to measure the force acting on NCs instead of STM tip.[64] The force value varied in a sawtooth pattern corresponding to the staircase pattern of conductance (Figure 7). It is supposed that the repetition of elastic and plastic regions appears in deformation process of Au NCs. In addition, force-displacement curve gives a spring constant of NCs.

In 2001, Kizuka et al. observed the deformation process of Au NCs using HRTEM-based *in situ* method with atomistic resolution. [65] They measured stress and strain quantitatively and started material mechanics research of metallic NCs. Using this method, mechanical properties of Cu[32], Ir[66], Pd[67], and Pt[51] NCs were researched. In 2005, Valkering et al. measured conductance and mechanical strength of Au and Pt NCs using developed tuning fork combined with MCBJ method. [68] As a result, force varied in a sawtooth pattern, which is similar to reference results. [63, 64].

1.4. Deformation of NCs

Sørensen et al. suggested three slip modes for deformation of NCs [69] (Figure 8). The tensile deformation axis is perpendicular to {111}. Deformation occurs with slipping on one, two, or three {111}, which are tilted from the tensile deformation axis (Figure 8).

To actually observe the deformation of NCs, two *in situ* HRTEM methods were developed; one is electron beam double holes drilling method. Electron beam drills two holes on material film with focused beam. A bridge that was formed between holes was gradually deformed using defocused electron beam.[70] The other method is the tip-sample contact method [65], and this fabricates and deforms NCs using piezo-driven tip. Kizuka and Tanaka observed Zn NCs using this method in HRTEM in 1994. [71] In 1997, Kizuka et al. directly observed the deformation process of Au NCs (Figure 9). [72] This is the first report that showed atomistic level observation of slip deformation process in crystals. After that, Ohnishi et al. fabricated Au NCs and observed deformation process from 5-atom width to 1-atom width in 1998. [73]

As Kizuka et al. further improved the *in situ* HRTEM method [74], they were able to observe the structural dynamics of NCs during tensile deformation process and research electrical and mechanical properties. [61] Until then, they were researched individually. They observed Au ASW at the final stage of tensile deformation process of Au NCs.

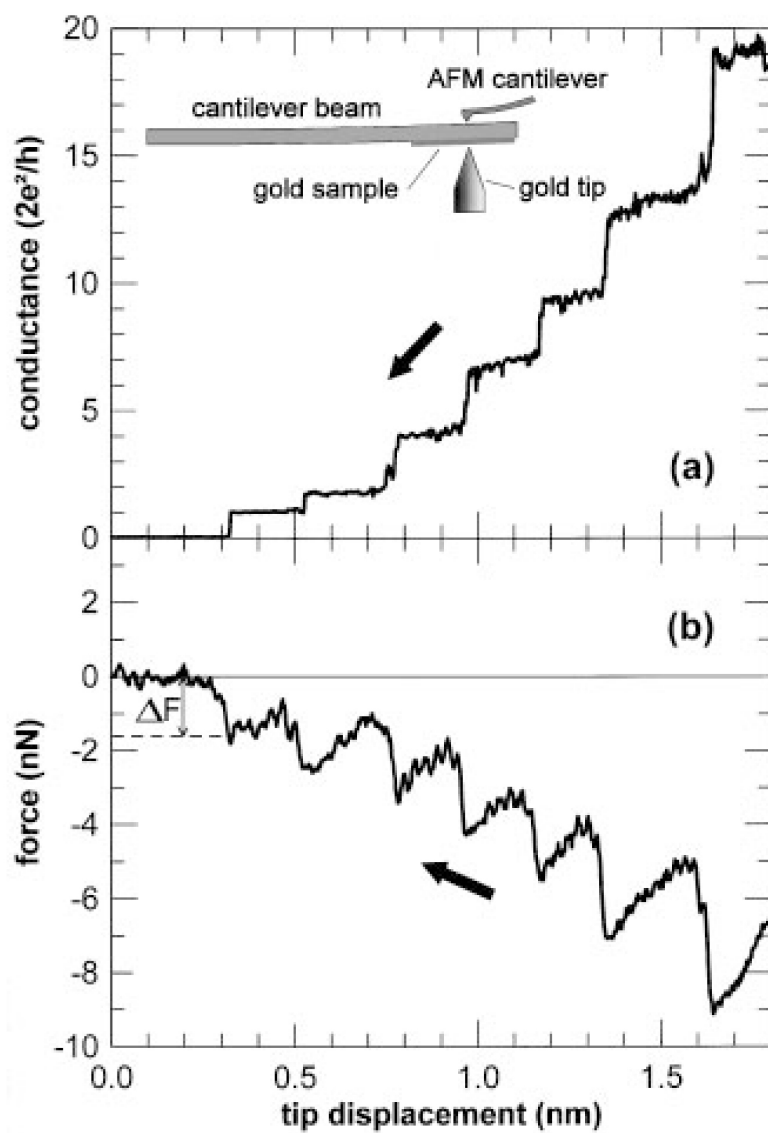


Figure 7. Conductance variation versus tip displacement in Au NCs measured by STM-AFM method.[64]

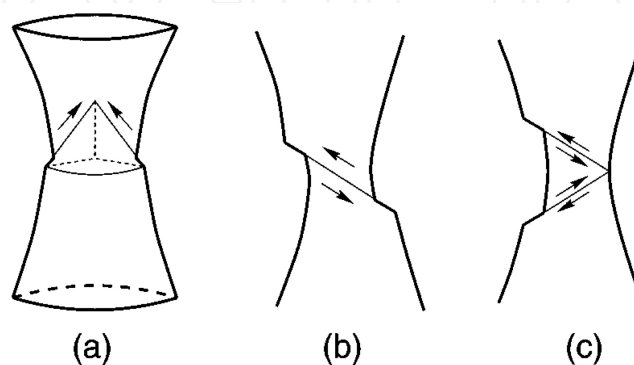


Figure 8. Deformation models of slip in Au NCs suggested by Sørensen et al.[69]

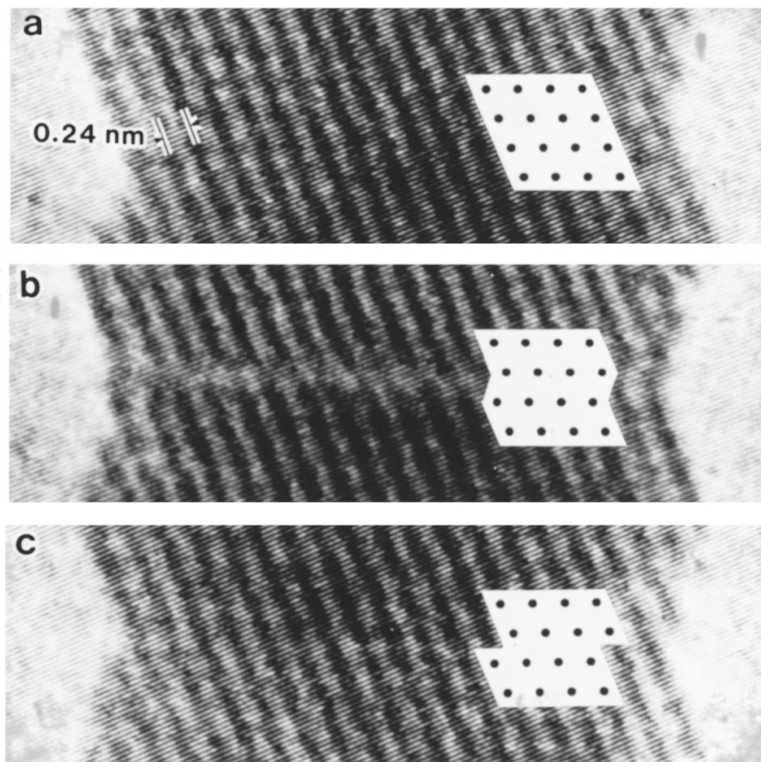


Figure 9. Time variation in elementary step of slip in shear deformation of Au NCs.[72]

The observed Au ASW has up to 10 atoms in length with an average interatomic distance of 0.27 nm (Figure 10). In tensile deformation process of ASWs, as tensile stress is concentrated on the contact region, interatomic distances of Au ASWs become longer up to 0.30 nm. At the same time, conductance of Au ASWs was measured. Resultant conductance greatly decreases when the number of atoms that is constructing ASWs exceed 4. Moreover, the force acting on the contact was measured. The tensile strength of this ASW was estimated to be from 8 to 17 GPa. This value is several times larger than that of Au NCs and much larger than bulk Au. At elastic deformation regions of stress-strain curves, Young's modulus of Au ASWs was estimated to be from 47 to 116 GPa. This value is remarkably comparable with that of single crystal Au.

The NCs and ASWs of other materials than Au have been also observed. The conductance quantization-type NCs, such as Au, Ag[26, 75] and Cu [34] ASWs, were also observed. On the other hand, those of anti-quantization-type NCs, such as Pt [47, 51], Pd[47, 76], Ir[66], and Co [47]ASWs, were also observed.

As described above, the problems in the research in metallic NCs commonly exist until now, among many materials as unrevealed below: 1) corresponding relationships between structure and electrical property of NCs, 2) phenomenon and mechanisms in the disappearance of conductance quantization, and 3) mechanical property of NCs. Especially, as research in NCs has been concentrated on Au, the structural dynamics of NCs is uncertain. Even some of the metallic NCs are already researched, only the structures that appeared in tensile deformation

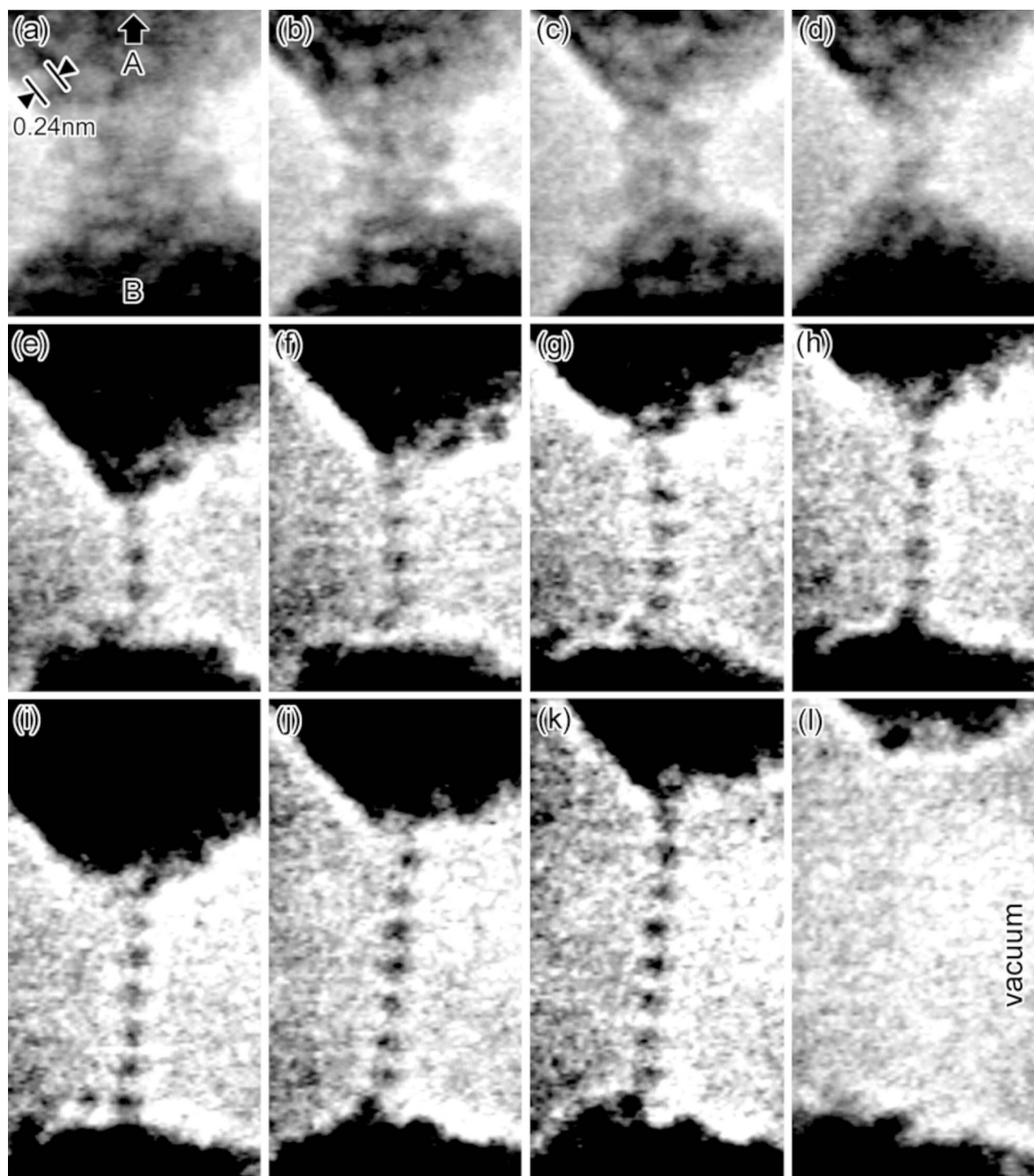


Figure 10. Time variation of Au ASW formation process observed by *in situ* HRTEM method.[61]

process have been observed. Therefore, the stable structure and electrical conductivity of the NCs are not yet revealed.

To guide the general rule of the phenomenon that appears in the metallic NCs, it is necessary to examine structural dynamics, electrical conductivity and mechanical properties, clarify the correspondence relationship between the structure and properties directly. The method used to observe structures and properties at the same time, which can analyse the correspondence, is limited *in situ* HRTEM method.

The purpose of this research is to clarify Ag NCs as a quantized metal using *in situ* HRTEM method. As Ag is expected to show the similar result as Au, statistical results are not observed.

2. *In situ* HRTEM

2.1. Experimental – *In situ* HRTEM -

In the observation of NCs, we used combined HRTEM with functions of STM and AFM (Figure 11) [61]. One can insert two specimen holders into the sample room of this microscopy. Each holder can be driven by a course mechanical goniometer that has ± 1 mm with submicron resolution and a fine piezo that has picometer scale. That is, we can move the sample to make a contact or a deformation with atomistic level using eight degrees of freedom.

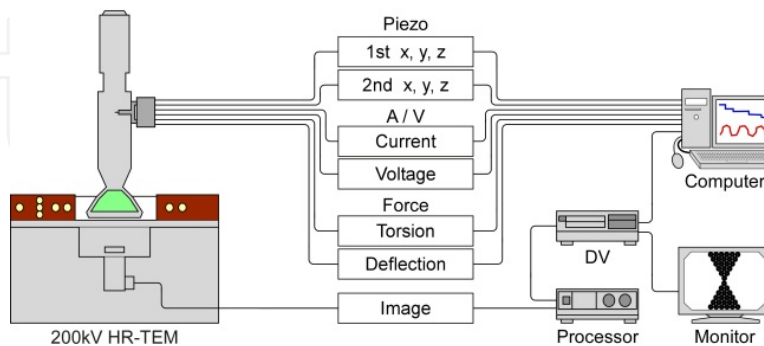
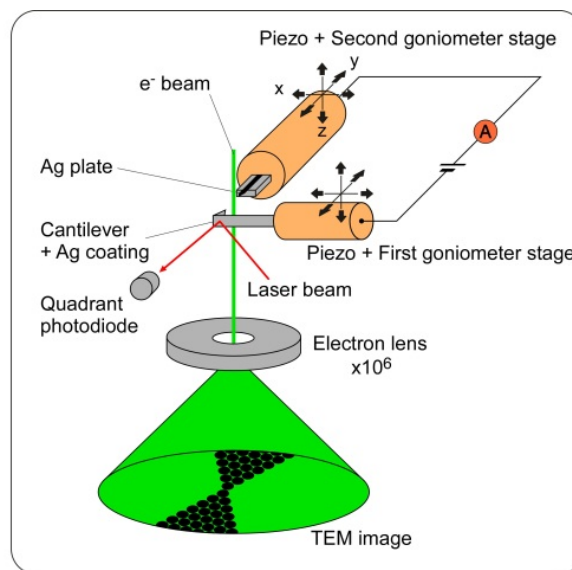


Figure 11. Schematic illustration of combined HRTEM.

When we measured the force acting on a contact, we attached a silicon cantilever used in AFM on one of the specimen holders. This cantilever was covered with metallic film that is 20-40 nm thick. The other one was mechanically polished and Ar-ion milled metallic thin plate.

HRTEM images were recorded with television camera. We applied bias voltages between samples. The current through the contact was measured by two-terminal method. The current signal was amplified 10^5 times and was then converted into voltage signal. Forces that are acting on a cantilever along deflection and torsion directions were detected using optical lever method used in AFM. When a laser is irradiated on the backside of cantilever, reflection angle of the laser varies with the cantilever deflection. We detected it as variation in relative strength of incident laser beam into quadrant photo-diode. These values were also amplified in the circuit. We recorded voltage signals corresponding to voltage, current, deflection, and torsion per 480 s, then we analysed these signals and observed images with time synchronizations.

Firstly, we set up two samples in a distance of 10 nm using course-moved mechanical goniometer with low magnification observation. After that, we made a contact using piezo drives. Then, we applied bias voltages of 13 mV and repeated to make a contact and tensile deformation. Each atomistic structure of NCs only appeared during several milliseconds in deformation process. This time is often shorter than the time resolution of the system of image recording for TEM (~ 17 ms / 1 frame). To observe specific structure longer, we used current to piezo drive feedback system.

3. Structure, conductance, and mechanical properties

3.1. Observation of tensile deformation process

In this section, we show the tensile deformation process of Ag NCs. Figure 12 is a time-sequence series of high-resolution images of the thinning process of Ag NC. The thinning was caused by the cantilever tip retraction from the plate with a speed of approximately 0.3 nm/s; the tip-plate distance was not controlled by the conductance feedback circuit in this observation. The tip and plate are observed with dark contrast in the upper and the lower regions of each frame, respectively. The NC is located at the centre of each image. The minimum cross section of the contacts is located in the middle of each frame between the tip and the plate in the vacuum. On the surfaces of both the tip and the plate, neither contamination nor an oxide layer is observed throughout Figs. 12(a)–12(f). The (111) lattice fringes with a 0.24 nm spacing are observed on the tip, the plate, and at their contact; the NC has a crystalline structure. The width of the minimum cross section in Fig. 12(a) is 2.2 nm. The width decreases as retraction proceeds, as shown in Figs. 12(b)–12(e). After this thinning, the width of the NC reaches 0.58 nm in Fig. 12(e), and finally, the NC breaks, as shown in Fig. 12(f).

Figure 13 is the time variation in strain, minimum cross-sectional area, current, current density, force, and stress of the Ag NC during the tip-plate retraction process shown in Fig. 12 as function of time. The time in Fig. 13 corresponds to the observation time in Fig. 12. As the tip-plate distance increases gradually, the minimum cross-sectional width decreases, as shown in Fig. 12(a) and 12(b). During this thinning process, rapid decreases in current and force are simultaneously observed. This shows that the thinning of the NC proceeds intermittently during tip retraction. Thus, slips occurred at these rapid decreases after elastic elongation, as indicated by the arrows above the force curve in Fig. 13. To calculate the current density and

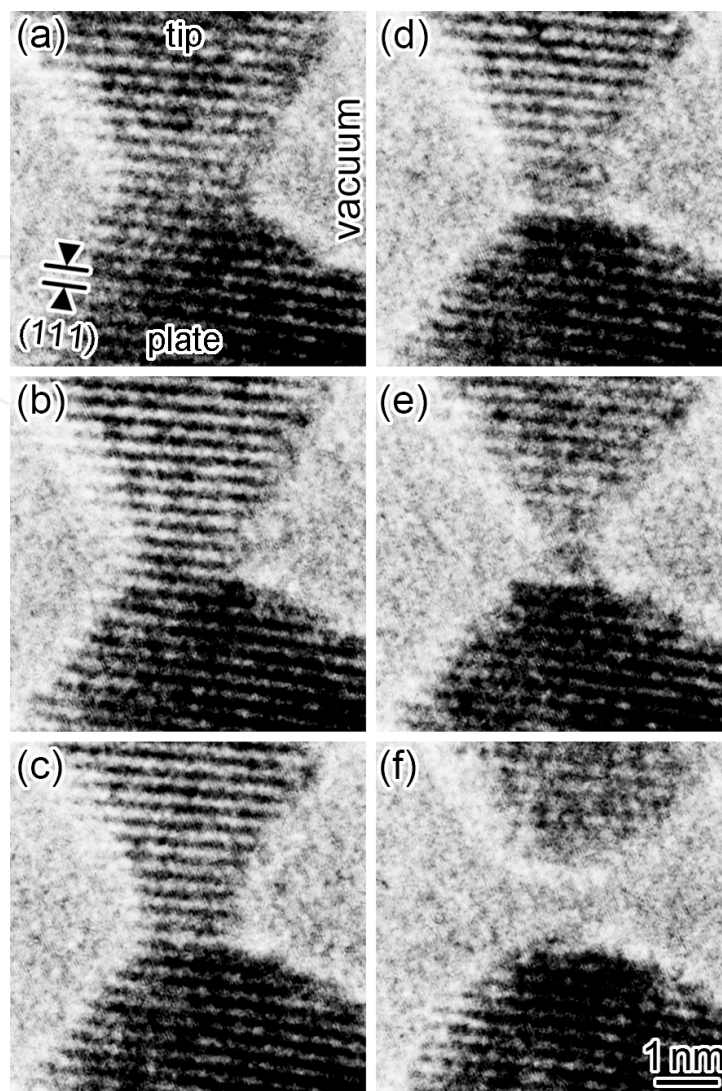


Figure 12. Time variation of HRTEM images in tensile deformation process of Ag NC. Bias voltage of 13 mV is applied. [77]

the stress of the NC, we assumed that the minimum cross section of the contact was circular. The minimum cross-sectional area was calculated using the observed width. In the time region from 0 to approximately 2.0 s, the stress increases as the cross-sectional area decreases.

The force at fracture is approximately 2 nN, which is similar to the values for Au single-atom contacts (approximately 1.5 nN).[64] The stress reaches approximately 3 GPa before fracture, which is 1/3 of the fracture strength previously observed for Au single-atom contacts (approximately 8 GPa)[61] and comparable to yield stress for Au NCs (1.7–4.2 GPa).[63] This shows that the critical shear stress of the Ag NC increases as the NC becomes thinner. The variation in stress against strain is represented in Fig. 14. A sawtooth curve, consisting of cycles of gradually increasing stress followed by a successive rapid decrease in stress is seen in Fig. 14. The regions of gradually increasing stress correspond to elastic elongation of the NC. The rapid decreases in the strain-stress curve correspond to slip events, due to the structural relaxation

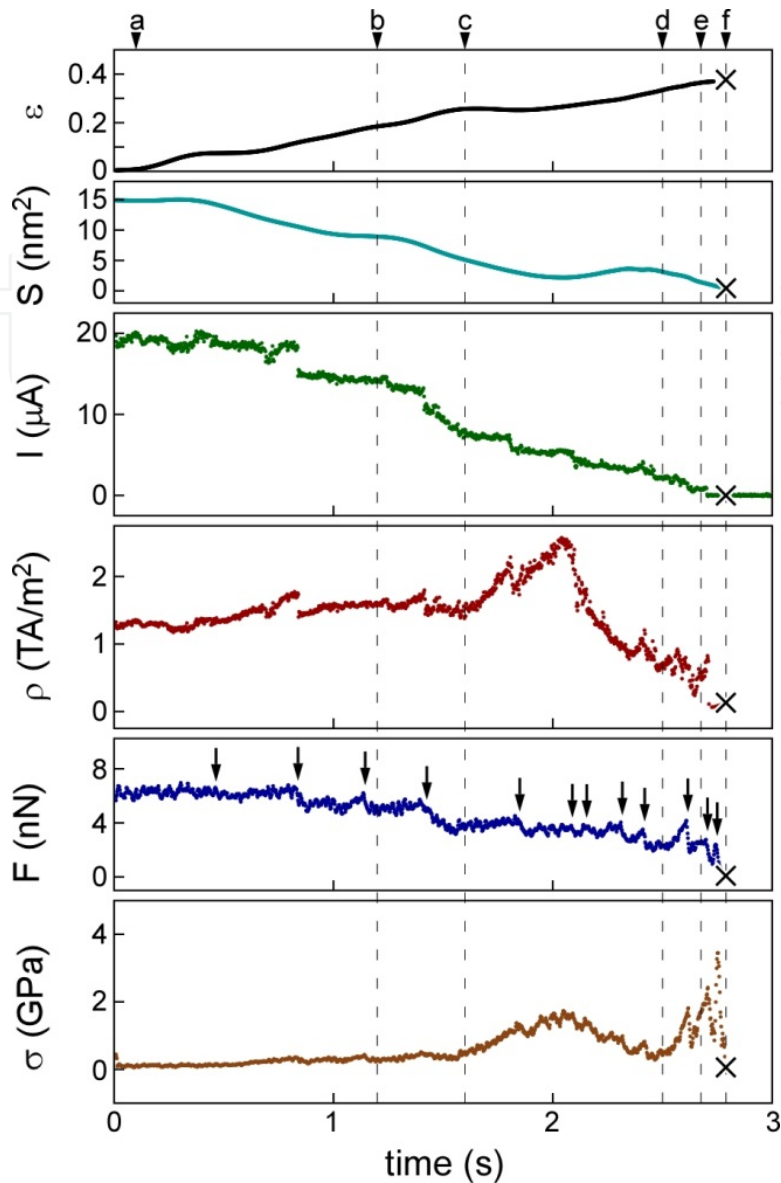


Figure 13. Time variation in strain, cross-sectional area, current, current density, force, and stress. Time is corresponding to Figure 12. Arrows corresponds to slip deformation of NC.[77]

of accumulated strain during elastic elongation. From the slope in each elastic elongation region, the plotted Young's modulus of the NC was estimated. Figure 15 shows the Young's modulus plotted against the minimum cross-sectional width. The slope changes at a width of approximately 1 nm.

3.2. Conductance histogram

Figure 16 shows the conductance of Ag NCs during the simple retraction of the tip. The histogram of the conductance values is integer multiples of G_0 . Figure 17 shows histograms of conductance values observed during feedback control. When the feedback value is assigned to be $1G_0$, one main peak is observed at the assigned value. For feedback values of 2 and

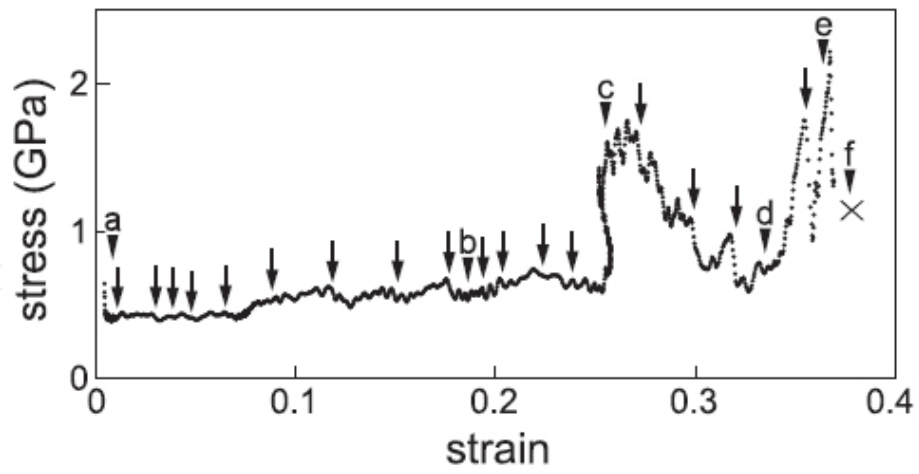


Figure 14. Stress-strain curve of Ag NC.[77]

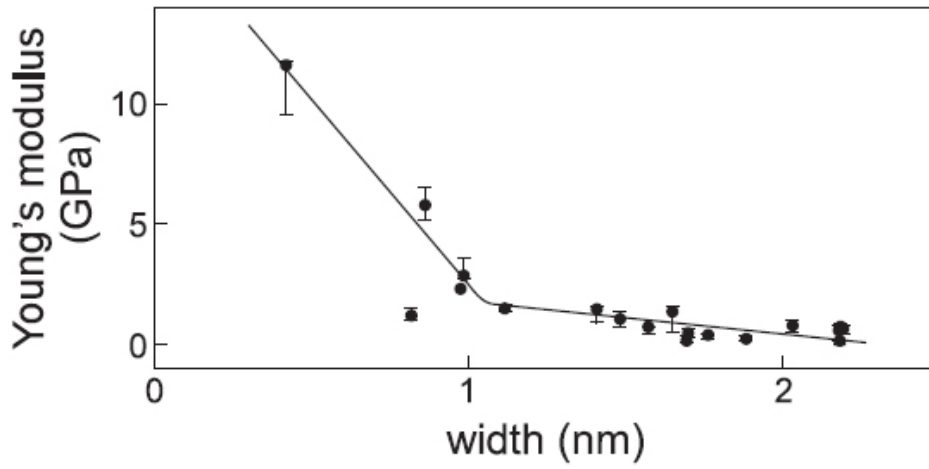


Figure 15. Young's modulus of Ag NC varied with width of contact.[77]

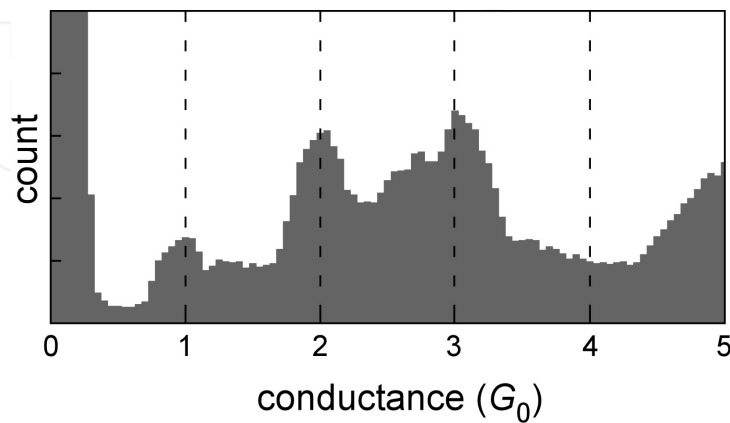


Figure 16. Conductance histograms accumulated from a plenty of tensile deformation process of Ag NCs.

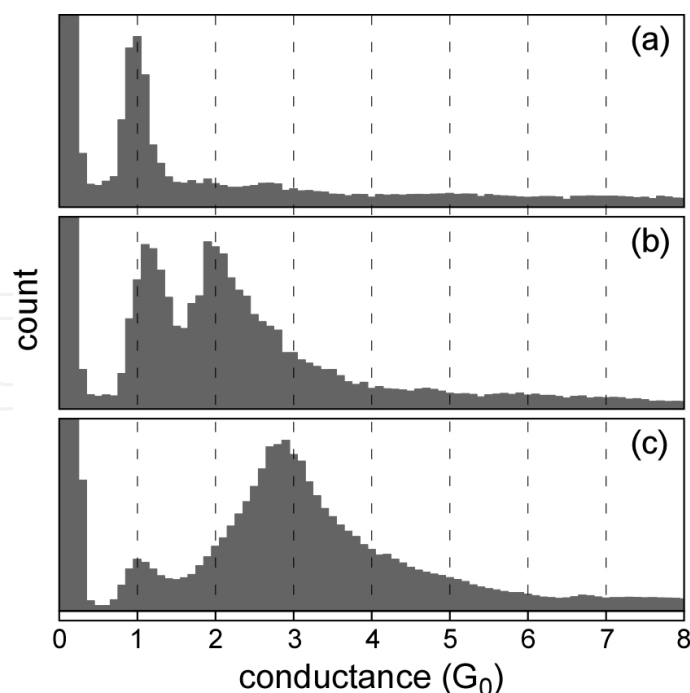


Figure 17. Conductance histograms of Ag NCs using current feedback system with bias voltage of 13 mV. Target conductance is (a) $1.0 G_0$, (b) $2.0 G_0$, and (c) $3.0 G_0$. [77]

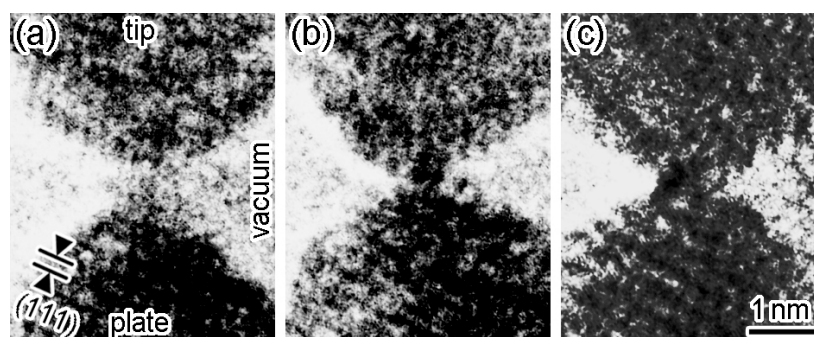


Figure 18. HRTEM images of Ag NCs using current feedback to $1 G_0$ with 13 mV. Minimum cross-sectional width is (a) 1-, (b) 2-, and (c) 3-atom. [77]

$3 G_0$, in addition to the main peak corresponding to the assigned value, another peak is observed at $1 G_0$.

Figure 18 shows high-resolution images of Ag contacts during conductance feedback control with an assigned value of $1 G_0$. As described for the high-resolution images in Fig. 12, the contacts are seen between the tip in the upper and the plate in the lower regions of each frame. The minimum cross-sectional widths of the contacts presented in Figs. 18(a)–18(c) are one, two, and three atoms, respectively. Thus, although the conductance value was the same, three types of contacts were observed. The $1 - G_0$ peaks in the conductance histograms arose from these types of contacts.

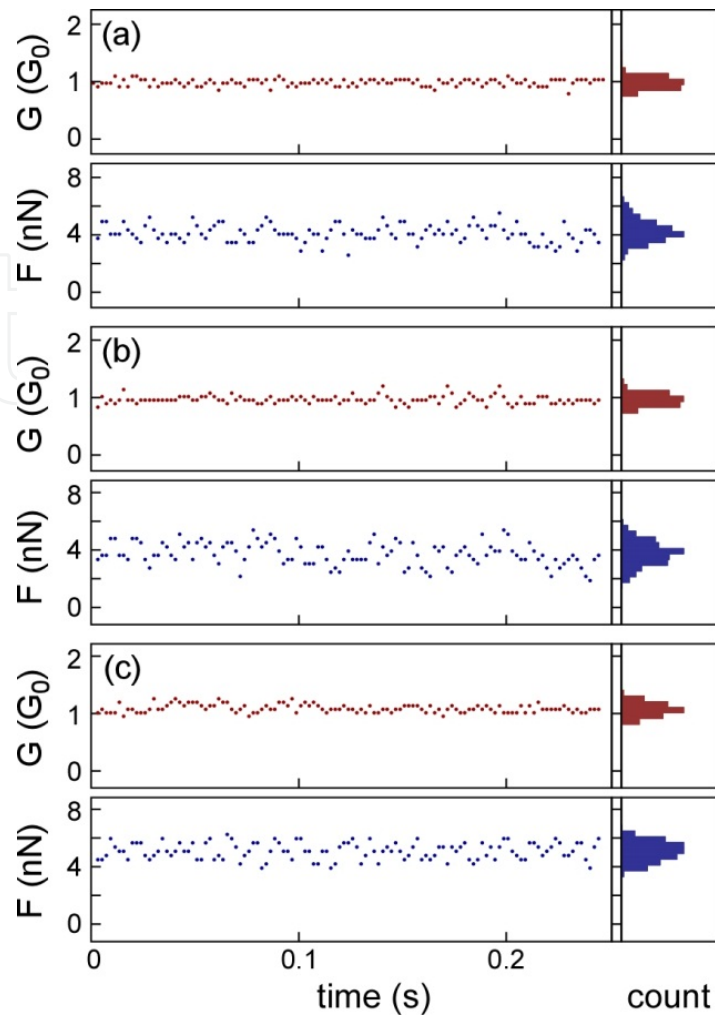


Figure 19. Conductance and force of Ag NCs under current feedback control.

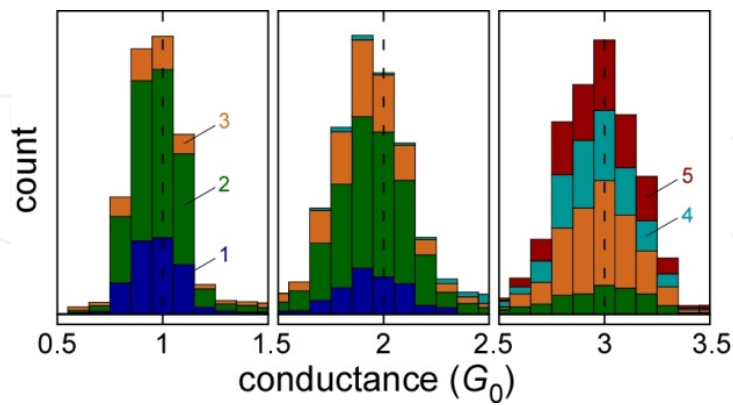


Figure 20. Conductance histograms of Ag NCs. Targets of current feedback system are $1 G_0$, $2 G_0$, and $3 G_0$. Each bin is coloured by cross-sectional width of NCs.

The contrast in Fig. 18 is weaker than that of Au NCs because the electron-scattering intensity of Ag atoms is lower than that of Au atoms.[61] Figures 19(a)–19(c) show the conductance of

and the force acting on the Ag contacts presented in Figs. 18(a)–18(c) during the conductance feedback control, respectively. The observed conductance values converged to be assigned a value of $1G_0$. The tensile force acting on each contact is 4.1 ± 1.0 nN for the single-atom contact [Fig. 19(a)], 4.0 ± 1.5 nN for the NC with a width of two atoms [Fig. 8(b)], and 5.3 ± 1.2 nN for the NC with a width of three atoms [Fig. 19(c)].

Figure 20 shows conductance histograms of the Ag contacts, along with their minimum cross-sectional width during feedback control with assigned values of conductance of 1, 2, and $3G_0$. The $1-G_0$ peak arose from contacts having widths of one, two, and three atoms with a counting ratio of 27%, 60%, and 13%, respectively. The $2-G_0$ and the $3-G_0$ peaks were generated by contacts having widths of one to four atoms and two to five atoms, respectively. For the $2G_0$ peak, the count ratio of the constituent contacts having width of one, two, three, and four atoms are 15%, 57%, 26%, and 3%, respectively. For the $3-G_0$ peak, the count ratio of the contacts having width of two, three, four, and five atoms are 12%, 36%, 26%, and 27%, respectively.

3.3. Mechanical properties of Ag NCs during thinning

The sawtooth curve was observed in the stress-strain relationship that is up to a strain of 0.25, as presented in Fig. 14. Thus, the tensile deformation of the NC initially proceeded through cycles of elastic elongation and subsequent slip up to this strain. The tensile stress at which the slips occurred was 0.5–0.6 GPa in the strain region of 0–0.25 in Fig. 3. The critical shear stress was calculated from the stress and the angle between the tensile and slip directions. The value calculated was 0.07 GPa, comparable to 1/10 of the theoretical shear stress (0.77 GPa) and the critical shear stress of Ag whiskers on {111} in $\langle 110 \rangle$ (0.71 GPa).[78] Thus, the slips in this strain region are inferred to be dislocation-mediated slips. After this slip process, a rapid increase in stress followed by a decrease is seen at a strain of 0.25. During the decrease, a sawtooth shape was observed: slip events continued after the rapid increase. The maximum stress in this region increased to 2 GPa. This stress corresponds to a critical shear stress of 0.2 GPa, comparable to 1/3 of the theoretical shear stress and whisker shear stress. It was also noted that for smaller contacts having widths of less than 1 nm, the slope of the Young's modulus-width relationship increased, and the modulus reached 10 GPa, as shown in Fig. 4. Thus, it is found that the elastic property of the NCs changes when their width decreases to less than 1 nm. These results reveal that a different type of deformation occurred for the smaller contacts. A molecular dynamics simulation by Sørensen et al. showed that in Au NCs, the crossover from a dislocation-mediated slip to a homogeneous slip occurs when their width decreases to less than 1.5 ± 0.3 nm.[69] In the present observation, the minimum cross-sectional width of the Ag NCs was 1.5 nm when the critical shear stress was 0.2 GPa. Therefore, it is inferred that the deformation mechanism changes from dislocation-mediated slip to homogeneous slip when the width decreases to less than 1.5 nm. That is, changes, such as increase in the Young's modulus of nanoscaled materials, are caused by a simplification of deformation system to a direct atomistic materials mechanics rather than a slip system of macroscaled materials. In such cases, mechanical properties of the materials are subject to modulation by the size effect.

3.4. Stable contact with a certain conductance

When the feedback value was assigned to be $1 G_0$, the observed conductance values converged to this assigned conductance, as shown in Fig. 6. On the other hand, when the feedback value was assigned to be other values, i.e., 2 and $3 G_0$, a $1 - G_0$ peak was observed in addition to the peak at each assigned value. In particular, when the assigned value was $2 G_0$, which is closer to $1 G_0$, the intensity of the $1 - G_0$ peak was comparable to that of the peak at $2 G_0$. This shows that the NCs exhibiting a conductance of $1 G_0$ were observed preferentially although the feedback control was performed to form NCs having other conductance; the stability of the $1 G_0$ NCs is higher than that of NCs exhibiting other conductance.

3.5. Structures of Ag NCs exhibiting a conductance of $1 G_0$

During the feedback control with an assigned conductance of $1 G_0$, three types of contacts, such as those with widths of one, two, and three atoms, were observed. In particular, we noted that in this feedback method, the contacts exhibiting a conductance of $1 G_0$ are not wires of single-atom width but of zero-length contacts. Therefore, single-atom-width Ag wires are less stable than the zero-length single-atom-width contacts in which the tip and plate are connected with one atom when they exhibit a conductance of $1 G_0$. It is pointed out, on the basis of theoretical analysis, tight binding, and free-electron calculations, that the conductance of metallic NCs and single-atom-width wires is sensitive to irregularities in the contact shape, a decrease in the convergent angle of electrodes, and small variation in the interatomic distance.[79-81] It was shown from a classical molecular dynamics simulation coupled with conductance calculations based on a tight binding model that the conductance of Ag NCs is sensitive to their atomic configuration and is not only determined by their width; for example, single-atom-width Ag contacts exhibit a conductance from 0.3 to $1.1 G_0$.[82] Thus, the present observation reveals that although the widths of the three types of contacts are different, their conductance becomes the same value, $1 G_0$, owing to this sensitivity. The force acting on the widest contacts, such as those with a width of three atoms, was larger than that acting on narrower contacts, such as NCs with width of one and two atoms. During feedback control, when the conductance of a NC was larger than the assigned value, the tip was manipulated to increase the tip-plate distance, resulting in the increase in force. It was reported that when tensile force acts on NCs during elastic elongation, the conductance decreases.[64] Thus, it is deduced that the conductance of the NC with a width of three atoms was decreased by the elongation due to the tensile force, and then the $1 G_0$ state was realized under this strained condition.

In the present study, in addition to simple tensile deformation, we introduced a conductance feedback system into *in situ* HRTEM to continuously observe Ag NCs exhibiting a certain conductance; in particular, we observed the quantized conductance values. Simultaneously, we measured the force acting on the contacts to investigate the stress of the NCs. From the observed structure and strain-stress relationship, it was found that the Young's modulus, which is, the elastic property of the NCs, changes when their width decreases to less than 1 nm. From the estimation of the critical shear stress of NCs, it was also inferred that the

deformation mechanism of NCs during thinning by simple retraction changes from dislocation-mediated slips to homogeneous slips when the width of NCs decreases to less than 1.5 nm. Using the conductance feedback system, it was found that several types of contacts with different widths contribute to the formation of each peak at the assigned conductance at quantized levels ($1 G_0$, $2 G_0$ and $3 G_0$) in the histogram. In particular, when the feedback conductance was assigned to be $1 G_0$, the contacts were not single-atom-width wires but three types of contacts, i.e., zero-length contacts with widths of one, two, and three atoms. Thus, it is concluded that such zero-length Ag contacts are more stable than single-atom-width Ag wires when they exhibit a conductance of $1 G_0$.

4. Current-voltage characteristics measurement

In this section, we show the current-voltage characteristics measurement of Ag NCs. Figure 21 is high-resolution images of the thinning process of Ag NC in a timeline. The NC is located at the centre of each image. The upper and the lower dark regions are the tip and the plate. The other brighter region is the vacuum. The continuous (111) lattice fringes of Ag (0.24 nm) are observed in the tip, the plate, and their contact region. It shows that the NC is a single crystalline structure. The width of the minimum cross section of the NC decreased from 6 atoms to 1 atom, and finally, the contact broke. Although the width of the contact region in Figs. 21(c) and 21(d) is the same, the contrast of the constricted region became brighter, implying that the thickness decreased. Figure 22 shows the high-resolution images and line profile of the constricted region of Figs. 21(d)–21(f). The intensity is classified into some levels; the intensities of the number of atom in thickness and the noise level in the vacuum. In Figs. 21(d) and 21(e), two and one large peaks are observed, indicating that their widths are 2 atoms and 1 atom, respectively. On the other hand, only the noise level is observed in the intensity in Fig. 21(f); the two tips are separated in the vacuum. From similar analysis, we constructed models of the atomic configurations of the Ag NC in Fig. 21, as shown in Fig. 22.

Figure 24 is the time-variation of the width, bias voltage, current, conductance, force, and stress during the thinning process of the Ag NC shown in Fig. 21, as a function of time. As the NC becomes thinner, the amplitude of the current and the conductance decrease stepwise. Similarly, the tensile force acting on the NC also decreases stepwise. The magnitude of the stress, which is calculated by dividing the force by the minimum cross-sectional area, is 1–6 GPa at times a–d and increases to 14 GPa before fracture at time e. Figure 25 shows the I–V curves measured for the NC presented in Fig. 21. The zero-bias conductance was estimated from the gradient of each curve to be $15 G_0$, $11 G_0$, $5 G_0$, $3 G_0$, and less than $0.1 G_0$, for the NC presented in Fig. 21, respectively. As previously analysed by Nielsen et al.,[84] we fitted the curves with third-order polynomials,

$$I_{total} = G^{(1)}V + G^{(2)}V^2 + G^{(3)}V^3 \quad (4)$$

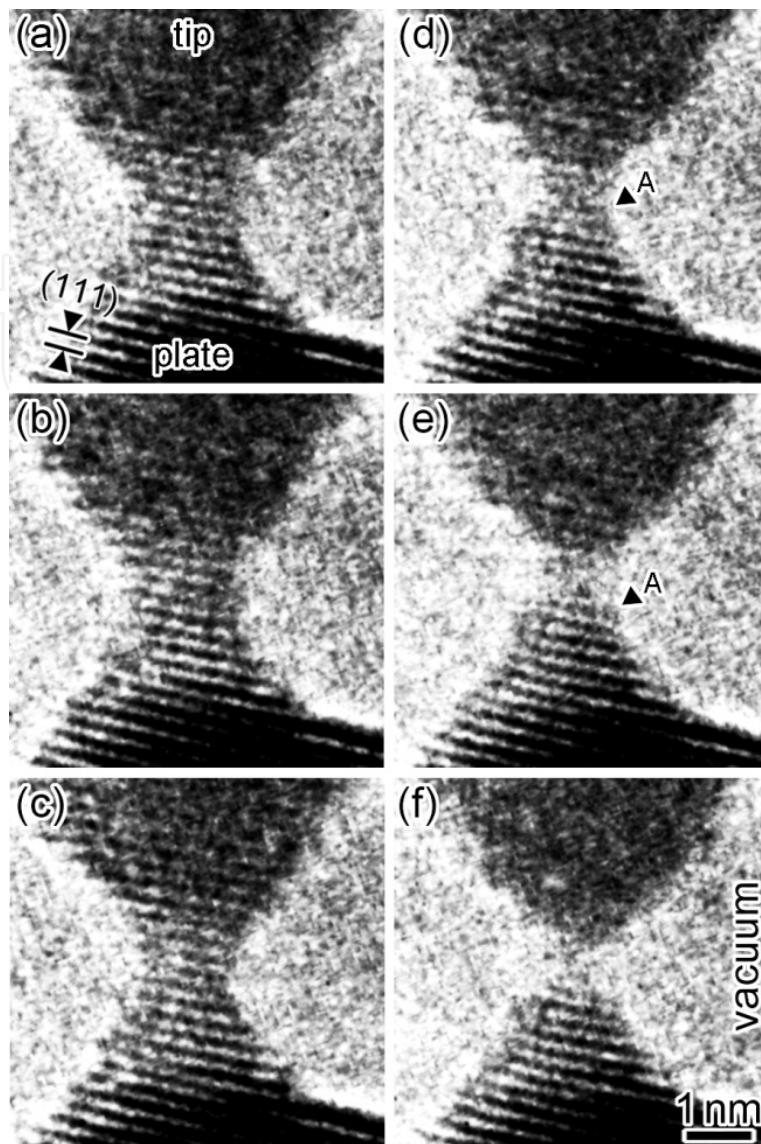


Figure 21. Time variation in HRTEM images of Ag NCs applying alternative current voltage of 13 mV.[83]

here, I_{total} is the current amount; V is the applied bias voltage; and $G^{(1)}V$, $G^{(2)}V^2$, and $G^{(3)}V^3$ are the coefficients of the first-, second-, and third-order-term that correspond to the conductance components – the lower bias voltages, the polarity dependence of the asymmetry of the contact structure, and the non-linearity, respectively. Figure 26 is the time variation of the non-linear parameter defined as $G^{(3)}/G^{(1)}$, and the ratio of the current of each term, $G^{(1)}V$, $G^{(2)}V^2$, and $G^{(3)}V^3$, to I_{total} as a function of conductance. The $G^{(1)}V$ component dominates the total current. For the NCs showing conductance larger than $10G_0$, both the $G^{(2)}V^2$ and $G^{(3)}V^3$ components show negative values; the total current is decreased from that in the case of linear I-V characteristics. For the NC of $3G_0$ (d in Fig. 26), the $G^{(2)}V^2$ component shows a positive value. The $G^{(3)}V^3$ component shows negative at states c and d in Fig. 26, whereas a positive value with an amount of 10% of the I_{total} was obtained at state e in Fig. 26. We compared

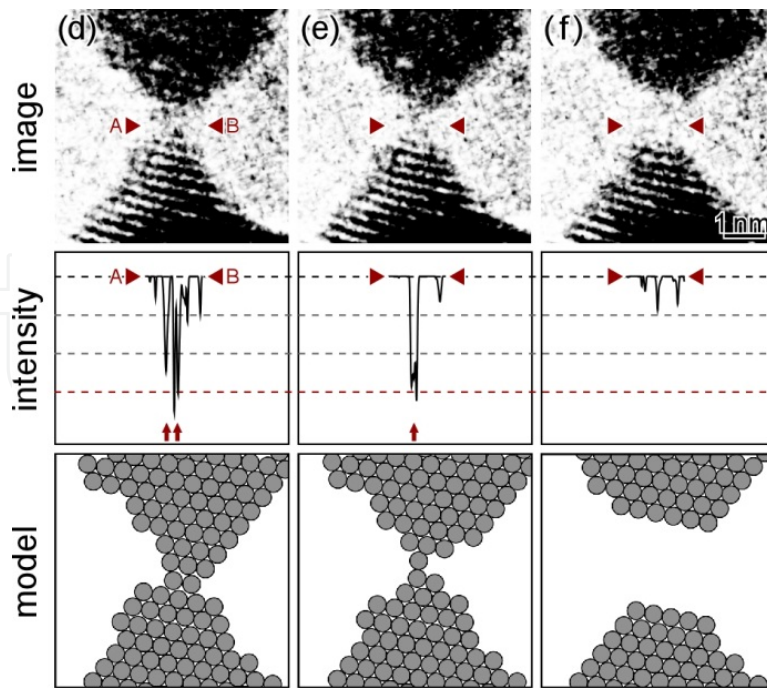


Figure 22. Atomistic configuration models of Ag NCs shown in Figure 21 (d-f).[83]

$G^{(3)}/G^{(1)}$ among those metallic NCs, i.e., Ag, Au, and Pt[51] NCs measured by the same method (Fig. 27).

4.1. Non-linearity of conductance and scattering of electrons in the Ag NC

The HRTEM images (shown in Fig. 21) were averaged over the time of 2 frames (over a period 67 ms), which is similar to one cycle of alternating bias voltage that is 50 ms (Fig. 24). Thus, one of the I–V curves was corresponding to the averaged image over the 1 period. We confirmed that no discernible changes in image were observed between the 2-frame images used for averaging in the television system. We also noted that there was no identified hysteresis in any of the I–V curves, and no change was observed between the successive increases and decreases in voltage. Under these conditions, the variation in the non-linear parameter was observed. Therefore, even though a small invisible structural change might occur and affect each I–V curve, the variation in the non-linear parameter was observed, which we discuss next. As shown in Fig. 26, $G^{(3)}V^3$ is negative, and its absolute value increases as the NC width decreases to 2 atoms (in Fig. 23). Thus, $G^{(3)}/G^{(1)}$ is also negative. As a result, the I–V curve deviates from a linear slope on the lower side, implying that electron scattering occurs in the NC. In this study, we selected the amplitude of the bias voltage of 13 mV, and no change in structure was observed during this bias application. At room temperature, the thermal energy is approximately 25 meV which is larger than the bias window used in this experiment. This thermal effect causes fluctuation in the I–V curves. However, because a tendency in the I–V curves was observed as the size of the NC decreased, we suppose that the parameters $G^{(2)}V^2$ and $G^{(3)}V^3$ contain certain information regarding the conduction nature.

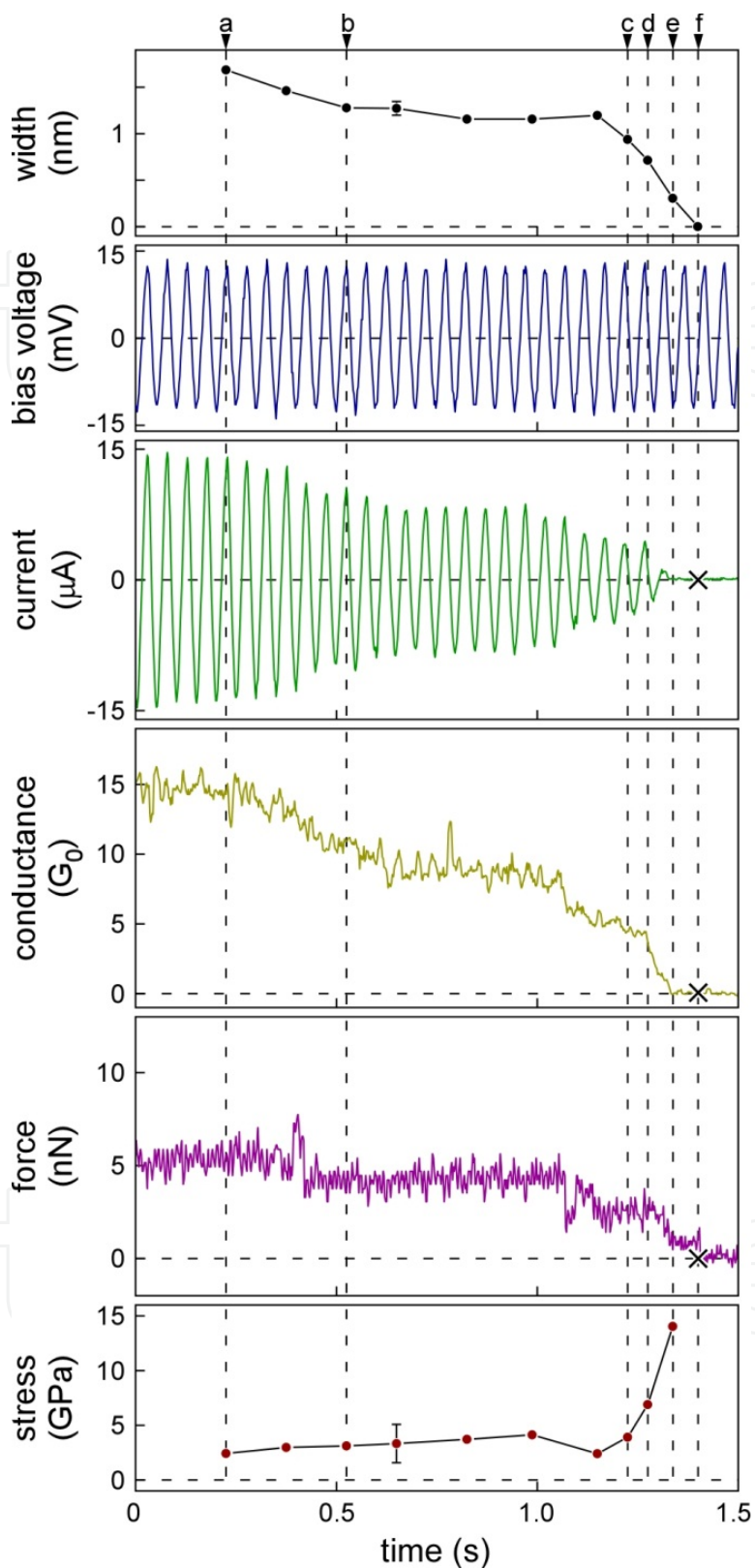


Figure 23. Time variation in width, applied bias, current, conductance, force, and stress of Ag NCs. Applied bias voltage is 20 Hz / 13 mV.

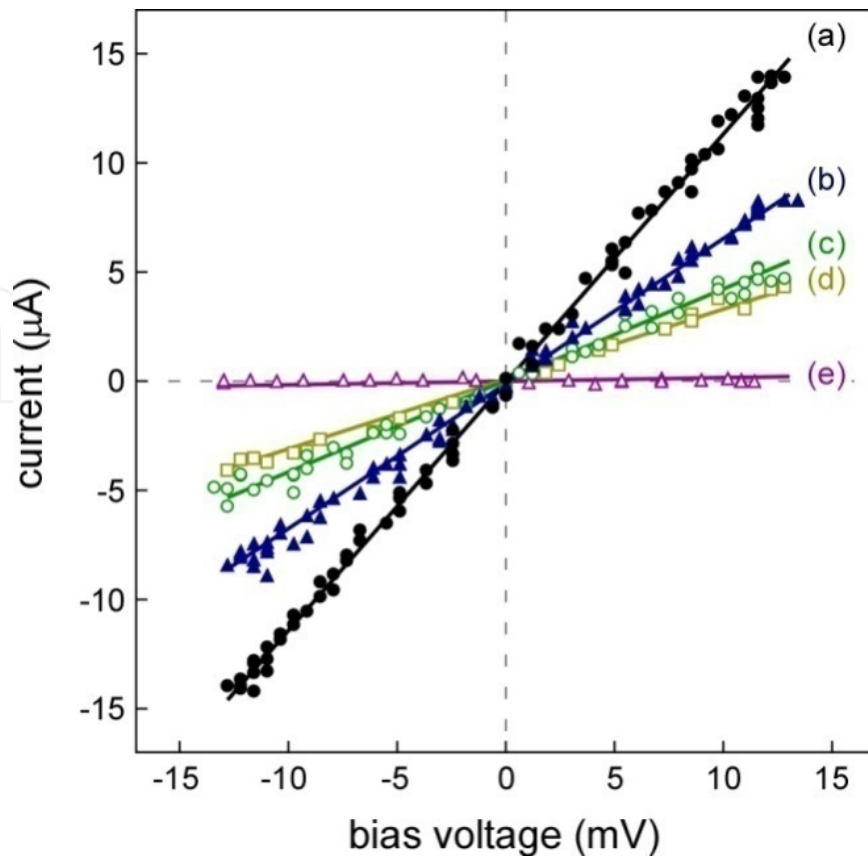


Figure 24. I-V curves of Ag NCs measured in Figure 21.

If we applied the bias voltage over 240 mV, the NCs of 5 nm size became unstable owing to electromigration; electron scattering increases enough to cause the atom migrations.[35] Such scattering contributes to the broadening of peaks in the conductance histograms of Ag NCs.[77]

As described above, electron scattering increases with decreasing contact width. During this thinning, the current density increased from 6 TA/m² (at time a) to 10 TA/m² (at time d). This current density was calculated by dividing the current value by the minimum cross-sectional area. On the other hand, when the contact transforms to the ASW, $G^{(3)} / G^{(1)}$ changes to positive. The current density of the ASW is 2 TA/m², which is a fifth of that of the 2-atom-width NC. These findings show that the density of states of the ASW differs from that of the NCs. As shown in Fig. 21, we could repeatedly observe the thinning of NCs to single-atom-contact. It was demonstrated that such contacts are sufficiently stable to analyse their I–V characteristics. However, we have confirmed that, in comparison with Au contacts, the stability of Ag contacts is lower. In particular, the formation probability of long ASWs in Ag is considerably lower. The smaller conductance of single-atom-width Ag contacts, observed in the present study, also shows the difference between Ag and Au single-atom-width contacts. Here, the result does not necessarily imply that the metal-insulator transition occurs in single-atom-width Ag contacts. This is because the current increases with the bias voltage even though the slope is lower than $0.1G_0$. At $0.1G_0$, the current corresponds to 100 nA at 13 mV, which is much larger than a tunnel current.

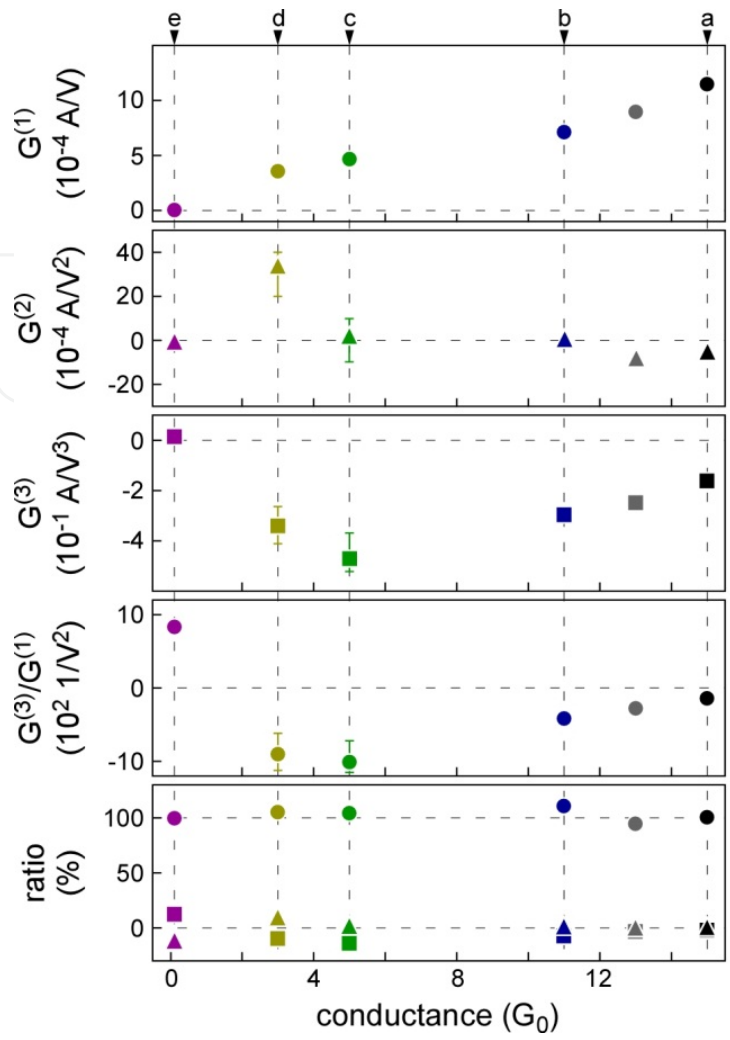


Figure 25. Fitting parameters of I-V curves.

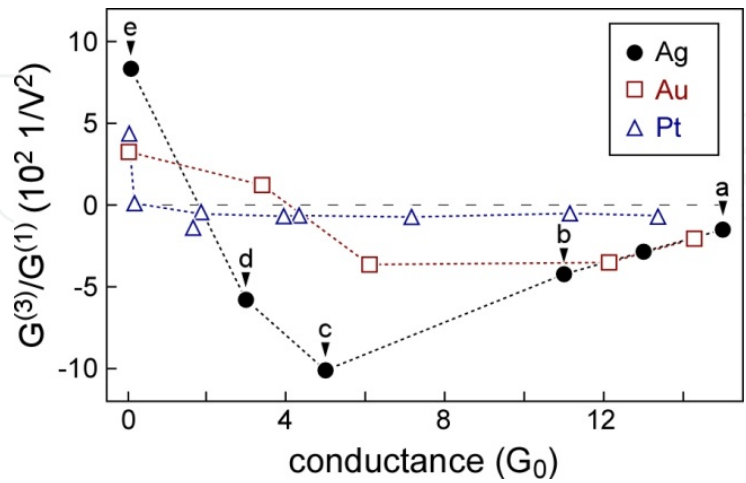


Figure 26. Non-linear parameter of metallic contacts.

4.2. Metal-specific differences

As shown in Fig. 26, $G^{(3)}/G^{(1)}$ in Ag and Au show similar variations; their $G^{(3)}/G^{(1)}$ values are negative and the absolute values increase with decreasing the width. The $G^{(3)}/G^{(1)}$ values of these ASWs have positive values. The $G^{(3)}/G^{(1)}$ values of Pt NCs are also negative: however, they are almost constant except for those of the ASW. This reflects that Ag and Au have s-like electronic structures, whereas Pt has a d-like electronic structure. Thus, the variation in the non-linear parameter $G^{(3)}/G^{(1)}$ depends on the valence electronic structure. We investigated the relationship between the structure and the I–V characteristics of Ag NCs. It was found that the non-linearity of conductance in Ag NCs increased with decreasing contact width. This tendency changed when the contact transformed to ASWs; the non-linear component became positive. The variation in the non-linear parameter of Ag NCs against conductance was similar to that of Au NCs, whereas it differed from that of Pt NCs. This feature corresponds to a feature in the electronic configuration of these elements.

5. Conclusions

In this study, we focused on Ag NCs and investigated the atomic arrangement, electrical conductivity and mechanical properties. In addition to the simple tensile deformation, particularly to observe the Ag NCs representing the certain conductance value of the quantized conductance, feedback circuit was introduced into *in situ* electron microscopy. At the same time, the measured stress and force acting on the NCs were estimated. The observed image and the stress-strain relationship gave us the elastic constant such as Young's modulus. It was found that to reduce the contact width below 1 nm, Young's modulus should be increased. From the value of the critical shear stress of Ag NCs, it is suggested that deformation mechanism changes to isotropic slip from a dislocation slip when the contact width decreases below 1.5 nm.

From the observation using a conductance feedback circuit, several types of NCs structures with different widths were found to contribute to a peak, which correspond to the quantization level in the conductance histograms. In particular, when conductance is controlled to $1 G_0$, the contact was 1-, 2-, and 3-atom width. From this fact, when the conductance indicates $1 G_0$, it is considered that Ag single atom contacts of zero length are more stable than the ASW structure.

As a result of I–V measurement of Ag NCs, non-linearity of the conductance increase when the width of the contacts reduces. When NCs deformed ASWs, this trend changes; non-linear components became positive. Changes of the conductance in non-linear parameters of Ag NCs are similar to that of Au and different from that of Pt. This corresponds to the characteristics of the valence electron configuration of the elements.

As described above, in this study, I examined the structure and properties of Ag NCs using *in situ* HRTEM method. The results of this study give us basic structure and properties that are the engineering basis in expanding the atomistic and molecular electronics in the future.

Acknowledgements

This work was partly supported by Japan Society for the Promotion of Science Fellows (No. 221479).

Author details

Hideki Masuda*

Address all correspondence to: MASUDA.Hideki@nims.go.jp

Advanced Key Technologies Division, National Institute for Materials Science, Tsukuba, Japan

References

- [1] Cuevas, JC, and Scheer, E: *Molecular electronics: an introduction to theory and experiment* (World Scientific, Singapore, 2010).
- [2] Joachim, C, Gimzewski, JK, and Aviram, A: Electronics using hybrid-molecular and mono-molecular devices. 2000; 408: 541. *Nature*.
- [3] Di Ventra, M, Pantelides, ST, and Lang, ND: First-principles calculation of transport properties of a molecular device. 2000; 84: 979. *Physical Review Letters*.
- [4] Kubatkin, S *et al.*: Single-electron transistor of a single organic molecule with access to several redox states. 2003; 425: 698. *Nature*.
- [5] Tao, NJ: Electron transport in molecular junctions. 2006; 1: 173. *Nature Nanotechnology*.
- [6] Danilov, A *et al.*: Electronic transport in single molecule junctions: control of the molecule-electrode coupling through intramolecular tunneling barriers. 2007; 8: 1. *Nano Letters*. 10.1021/nl071228o.
- [7] Kim, WY *et al.*: Application of quantum chemistry to nanotechnology: electron and spin transport in molecular devices. 2009; 38: 2319. *Chemical Society Reviews*.
- [8] Masuda, H, and Kizuka, T: Distance control of electromigration-induced silver nanogaps. 2014; 14: 2436. *Journal of Nanoscience and Nanotechnology*. doi:10.1166/jnn.2014.8502.
- [9] van Wees, BJ *et al.*: Quantized conductance of point contacts in a two-dimensional electron gas. 1988; 60: 848. *Physical Review Letters*.

- [10] Agraït, N, Yeyati, AL, and van Ruitenbeek, JM: Quantum properties of atomic-sized conductors. 2003; 377: 81. Physics Reports.
- [11] Olesen, L *et al.*: Quantized conductance in an atom-sized point contact. 1994; 72: 2251. Physical Review Letters.
- [12] Muller, CJ, van Ruitenbeek, JM, and de Jongh, LJ: Conductance and supercurrent discontinuities in atomic-scale metallic constrictions of variable width. 1992; 69: 140. Physical Review Letters.
- [13] Ludoph, B *et al.*: Multiple Andreev reflection in single-atom niobium junctions. 2000; 61: 8561. Physical Review B.
- [14] Oshima, H, and Miyano, K: Spin-dependent conductance quantization in nickel point contacts. 1998; 73: 2203. Appl. Phys. Lett..
- [15] Scheer, E *et al.*: The signature of chemical valence in the electrical conduction through a single-atom contact. 1998; 394: 154. Nature.
- [16] Costa-Krämer, JL *et al.*: Nanowire formation in macroscopic metallic contacts: quantum mechanical conductance tapping a table top. 1995; 342: L1144. Surface Science.
- [17] Costa-Krämer, JL: Conductance quantization at room temperature in magnetic and nonmagnetic metallic nanowires. 1997; 55: R4875. Physical Review B.
- [18] Krans, JM *et al.*: The signature of conductance quantization in metallic point contacts. 1995; 375: 767. Nature.
- [19] Fujii, A *et al.*: Break conductance of noble metal contacts. 2005; 72: 045407. Physical Review B.
- [20] Rodrigues, V, Fuhrer, T, and Ugarte, D: Signature of atomic structure in the quantum conductance of gold nanowires. 2000; 85: 4124. Physical Review Letters.
- [21] Ludoph, B, and van Ruitenbeek, JM: Conductance fluctuations as a tool for investigating the quantum modes in atomic-size metallic contacts. 2000; 61: 2273. Physical Review B.
- [22] Untiedt, C *et al.*: Formation of a metallic contact: jump to contact revisited. 2007; 98: 206801. Physical Review Letters.
- [23] Thijssen, WHA *et al.*: Oxygen-enhanced atomic chain formation. 2006; 96: 026806. Physical Review Letters.
- [24] Mares, AI, and van Ruitenbeek, JM: Observation of shell effects in nanowires for the noble metals Cu, Ag, and Au. 2005; 72: 205402. Physical Review B.
- [25] Liang, J *et al.*: Correlating conductance and structure of silver nano-contacts created by jump-to-contact STM break junction. 2013; 688: 257. Journal of Electroanalytical Chemistry.

- [26] Rodrigues, V *et al.*: Quantum conductance in silver nanowires: Correlation between atomic structure and transport properties. 2002; 65: 153402. *Physical Review B*.
- [27] Li, CZ, and Tao, NJ: Quantum transport in metallic nanowires fabricated by electrochemical deposition/dissolution. 1998; 72: 894. *Applied Physics Letters*.
- [28] Krans, JM *et al.*: One-atom point contacts. 1993; 48: 14721. *Physical Review B*.
- [29] Li, CZ *et al.*: Fabrication of stable metallic nanowires with quantized conductance. 1999; 10: 221. *Nanotechnology*.
- [30] Bakker, DJ *et al.*: Effect of disorder on the conductance of a Cu atomic point contact. 2002; 65: 235416. *Physical Review B*.
- [31] Li, J *et al.*: Metal-dependent conductance quantization of nanocontacts in solution. 2002; 81: 123. *Applied Physics Letters*.
- [32] Fujisawa, S, Kikkawa, T, and Kizuka, T: Direct observation of electromigration and induced stress in Cu nanowire. 2003; 42: L1433. *Japanese Journal of Applied Physics*.
- [33] Fujii, A *et al.*: High-bias conductance of atom-sized Cu contacts. 2004; 464-465: 251. *Thin Solid Films*. <http://dx.doi.org/10.1016/j.tsf.2004.06.033>.
- [34] González, JC *et al.*: Indication of unusual pentagonal structures in atomic-size Cu nanowires. 2004; 93: 126103. *Physical Review Letters*.
- [35] Kizuka, T, and Aoki, H: The dynamics of electromigration in copper nanocontacts. 2009; 2: 075003. *Applied Physics Express*.
- [36] Yanson, AI, Yanson, IK, and van Ruitenbeek, JM: Observation of shell structure in sodium nanowires. 1999; 400: 144. *Nature*.
- [37] Sim, HS, Lee, HW, and Chang, KJ: Even-odd behavior of conductance in monatomic sodium wires. 2001; 87: 096803. *Physical Review Letters*.
- [38] Muller, CJ, van Ruitenbeek, JM, and de Jongh, LJ: Experimental observation of the transition from weak link to tunnel junction. 1992; 191: 485. *Physica C: Superconductivity*. [http://dx.doi.org/10.1016/0921-4534\(92\)90947-B](http://dx.doi.org/10.1016/0921-4534(92)90947-B).
- [39] Sirvent, C *et al.*: STM study of the atomic contact between metallic electrodes. 1996; 218: 238. *Physica B: Condensed Matter*.
- [40] García, N, Muñoz, M, and Zhao, YW: Magnetoresistance in excess of 200% in ballistic Ni nanocontacts at room temperature and 100 Oe. 1999; 82: 2923. *Physical Review Letters*.
- [41] Ono, T *et al.*: $2e^2/h$ to e^2/h switching of quantum conductance associated with a change in nanoscale ferromagnetic domain structure. 1999; 75: 1622. *Applied Physics Letters*.

- [42] Sirvent, C *et al.*: Conductance step for a single-atom contact in the scanning tunneling microscope: Noble and transition metals. 1996; 53: 16086. *Physical Review B*.
- [43] Yuki, K, Shu, K, and Akira, S: Quantized conductance in Pt nanocontacts. 2000; 39: 4593. *Japanese Journal of Applied Physics*.
- [44] Yuki, K, Kurokawa, S, and Sakai, A: Conductance in breaking nanocontacts of some transition metals. 2001; 40: 803. *Japanese Journal of Applied Physics*.
- [45] Smit, RHM *et al.*: 2002; 419: 906. *Nature*.
- [46] Smit, RHM *et al.*: Observation of a parity oscillation in the conductance of atomic wires. 2003; 91: 076805. *Physical Review Letters*.
- [47] Rodrigues, V *et al.*: Evidence for spontaneous spin-polarized transport in magnetic nanowires. 2003; 91: 096801. *Physical Review Letters*.
- [48] Nielsen, SK *et al.*: Conductance of single-atom platinum contacts: Voltage dependence of the conductance histogram. 2003; 67: 245411. *Physical Review B*.
- [49] Csonka, S *et al.*: Conductance of Pd-H Nanojunctions. 2004; 93: 016802. *Physical Review Letters*.
- [50] Djukic, D *et al.*: Stretching dependence of the vibration modes of a single-molecule Pt-H[₂]-Pt bridge. 2005; 71: 161402. *Physical Review B*.
- [51] Kizuka, T, and Monna, K: Atomic configuration, conductance, and tensile force of platinum wires of single-atom width. 2009; 80: 205406. *Physical Review B*.
- [52] Yanson, AI, and van Ruitenbeek, JM: Do histograms constitute a proof for conductance quantization? 1997; 79: 2157. *Physical Review Letters*.
- [53] Mizobata, J-i *et al.*: High-bias conductance of atom-sized Al contacts. 2003; 68: 155428. *Physical Review B*.
- [54] Smit, RHM *et al.*: Common origin for surface reconstruction and the formation of chains of metal atoms. 2001; 87: 266102. *Physical Review Letters*.
- [55] Minowa, T *et al.*: Conductance of Pd single-atom contacts. 2005; 241: 14. *Applied Surface Science*. <http://dx.doi.org/10.1016/j.apsusc.2004.09.010>.
- [56] Suzuki, R *et al.*: Conductance of atom-Sized Zn contacts. 2006; 45: 7217. *Japanese Journal of Applied Physics*.
- [57] Tsutsui, M, Kurokawa, S, and Sakai, A: Bias-induced local heating in atom-sized metal contacts at 77 K. 2007; 90: 133121. *Applied Physics Letters*.
- [58] Post, N, and Ruitenbeek, JM: High stability STM made of a break junction. 1996; 46: 2853. *Czechoslovak Journal of Physics*. [10.1007/bf02570413](https://doi.org/10.1007/bf02570413).
- [59] Landauer, R: 1988; 32: 306. *IBM Journal of Research and Development*.

- [60] Sharvin, YV: 1965; 48: 984. Zhurnal Eksperimental'noi i Teoreticheskoi Fiziki.
- [61] Kizuka, T: Atomic configuration and mechanical and electrical properties of stable gold wires of single-atom width. 2008; 77: 155401. Physical Review B.
- [62] Gimzewski, JK, and Möller, R: Transition from the tunneling regime to point contact studied using scanning tunneling microscopy. 1987; 36: 1284. Physical Review B.
- [63] Agraït, N, Rubio, G, and Vieira, S: Plastic deformation of nanometer-scale gold connective necks. 1995; 74: 3995. Physical Review Letters.
- [64] Rubio, G, Agraït, N, and Vieira, S: Atomic-sized metallic contacts: mechanical properties and electronic transport. 1996; 76: 2302. Physical Review Letters.
- [65] Kizuka, T *et al.*: Simultaneous observation of millisecond dynamics in atomistic structure, force and conductance on the basis of transmission electron microscopy 2001; 40: L170. Japanese Journal of Applied Physics.
- [66] Ryu, M, and Kizuka, T: Structure, conductance and strength of iridium wires of single atom Width 2006; 45: 8952. Japanese Journal of Applied Physics.
- [67] Matsuda, T, and Kizuka, T: Structure of nanometer-sized palladium contacts and their mechanical and electrical properties 2007; 46: 4370. Japanese Journal of Applied Physics.
- [68] Valkering, AMC *et al.*: A force sensor for atomic point contacts. 2005; 76: 103903. Review of Scientific Instruments.
- [69] Sørensen, MR, Brandbyge, M, and Jacobsen, KW: Mechanical deformation of atomic-scale metallic contacts: Structure and mechanisms. 1998; 57: 3283. Physical Review B.
- [70] Kondo, Y, and Takayanagi, K: Gold nanobridge stabilized by surface structure. 1997; 79: 3455. Physical Review Letters.
- [71] Kizuka, T, and Tanaka, N: Dynamic high-resolution electron microscopy of diffusion bonding between zinc oxide nanocrystallites at ambient temperature 1994; 69: 135. Philosophical Magazine Letters.
- [72] Kizuka, T: Atomistic visualization of deformation in gold. 1998; 57: 11158. Physical Review B.
- [73] Ohnishi, H, Kondo, Y, and Takayanagi, K: Quantized conductance through individual rows of suspended gold atoms 1998; 395: 780. Nature.
- [74] Kizuka, T, Umehara, S, and Fujisawa, S: Metal-insulator transition in stable one-dimensional arrangements of single gold atoms 2001; 40: L71. Japanese Journal of Applied Physics.
- [75] Lagos, MJ *et al.*: Observation of the smallest metal nanotube with a square cross-section. 2009; 4: 149. Nature Nanotechnology.

- [76] Matsuda, T, and Kizuka, T: Palladium wires of single atom width as mechanically controlled switching devices 2006; 45: L1337. Japanese Journal of Applied Physics.
- [77] Masuda, H, and Kizuka, T: Structure, electrical, and mechanical properties of silver nanocontacts. 2010; 49: 045202. Japanese Journal of Applied Physics.
- [78] Kelley, A, *Strong Solid* (Clarendon Press, Oxford, 1966).
- [79] Bratkovsky, AM, Sutton, AP, and Todorov, TN: Conditions for conductance quantization in realistic models of atomic-scale metallic contacts. 1995; 52: 5036. Physical Review B.
- [80] Scherbakov, AG, Bogachek, EN, and Landman, U: Quantum electronic transport through three-dimensional microconstrictions with variable shapes. 1996; 53: 4054. Physical Review B.
- [81] Todorov, TN, and Sutton, AP: Jumps in electronic conductance due to mechanical instabilities. 1993; 70: 2138. Physical Review Letters.
- [82] Pauly, F *et al.*: Theoretical analysis of the conductance histograms and structural properties of Ag, Pt, and Ni nanocontacts. 2006; 74: 235106. Physical Review B.
- [83] Masuda, H, and Kizuka, T: Current-voltage characteristics of silver nanocontacts studied by *in situ* transmission electron microscopy. 2012; 81: 114707. Journal of Physical Society of Japan. 10.1143/JPSJ.81.114707.
- [84] Nielsen, SK *et al.*: Current-voltage curves of atomic-sized transition metal contacts: an explanation of why Au is ohmic and Pt is not. 2002; 89: 066804. Physical Review Letters.

